Piezoelectric InAs (211)B quantum dots grown by molecular beam epitaxy: Structural and optical properties

G. E. Dialynas,[1,a)] S. Kalliakos,[2] C. Xenogianni,[2] M. Androulidaki,[3] T. Kehagias,[4] P. Komninou,[4] P. G. Savvidis,[2,3] Z. Hatzopoulos,[1,3] and N. T. Pelekanos[2,3]
[1]*Department of Physics, University of Crete, P.O. Box 2208, 71003 Heraklion, Greece*
[2]*Department of Materials Science and Technology, University of Crete, P.O. Box 2208, 71003 Heraklion, Greece*
[3]*Microelectronics Research Group, IESL-FORTH, P.O. Box 1385, 71110 Heraklion, Greece*
[4]*Department of Physics, Aristotle University of Thessaloniki, 54124 Thessaloniki, Greece*

(Received 14 May 2010; accepted 2 October 2010; published online 30 November 2010)

The structural and optical properties of piezoelectric (211)B InAs nanostructures grown by molecular beam epitaxy are systematically investigated as a function of the various growth parameters. Depending on the specific growth conditions, we show that the InAs nanostructures take the form of a quantum dot (QD) or a quantum dash, their height ranges between 2 and 20 nm, and their density varies from a few times 10^8 cm^{-2} all the way up to a few times 10^{10} cm^{-2}. The (211)B QDs are characterized by large aspect ratios, which are compatible with a truncated pyramid morphology. By analyzing the QD emission spectrum, we conclude that only small size QDs, with heights less than 3 nm, are optically active. This is consistent with high resolution transmission electron microscopy observations showing that large QDs contain misfit dislocations, whereas small QDs are dislocation-free. The formation of a two-dimensional wetting layer is observed optically, and its thickness is determined to be between 0.30 and 0.39 nm. Finally, the large blueshift in the QD emission observed with increasing excitation power represents a clear evidence of the strong built-in piezoelectric field present in these dots. © *2010 American Institute of Physics*.
[doi:10.1063/1.3510490]

I. INTRODUCTION

During the past fifteen years, a vast amount of research has been devoted to the study of electronic and optical properties of InAs quantum dots (QDs), motivated in part by their potential for improved optoelectronic devices, but also by the fact that QDs are an excellent study-case of quantum effects in the nanoscale.[1–4] So far, the large majority of studies have focused on InAs QDs grown on (100)-oriented GaAs substrates, whereas only few were devoted to other crystalline orientations.[5–9] It has been known for some time that the substrate orientation strongly affects the growth kinetics of the InAs/GaAs heteroepitaxy. The distinct surface atomic structures of the different crystalline orientations modify the adsorption, migration, and desorption of adatoms on the growing surface, as well as the strain relaxation mechanisms taking part during the QD formation. Hence, substrate orientation can strongly affect the structural and optical properties of the grown QDs.

Another interesting aspect of InAs nanostructures grown on high index GaAs surfaces is the possibility for large strain-induced piezoelectric (PZ) fields, whose magnitude are strongly dependent on substrate orientation and lattice mismatch.[10] Experimental evidence for the existence of large PZ fields in (N11) InAs QDs has been reported previously.[11,12] By using bulk InAs PZ coefficients, a PZ field of 250 kV/cm was estimated for (211) InAs QDs.[11] For comparison, we note that this value is a small fraction of the 7 MV/cm internal field observed in hexagonal c-axis oriented GaN QDs.[13,14] However, recent *ab initio* theoretical calculations of PZ coefficients in highly-strained InAs suggest that the PZ field in (N11) InAs QDs is strongly enhanced by nonlinear PZ effects, and can reach values in excess of 1 MV/cm for (211) InAs QDs.[15] Such strong fields are expected to dominate the optical and dynamic properties of (N11) InAs QDs.

High index InAs nanostructures offer unique advantages and can lead to many exciting applications. For instance, InGaAs QDs grown on high index substrates have exhibited superior optical properties compared to (100) counterparts.[5] Moreover, high index surfaces were found to provide increased control of spatial ordering of the QDs compared to the (100) GaAs surface.[16] Furthermore, laser diodes using (111)B InGaAs/GaAs quantum wells have been shown to outperform their (100) counterparts in terms of reduced threshold currents,[17] an advantage likely to be transferable to low threshold QD laser diodes using high index QDs. The main motivation, however, for the renewed interest in (N11) InAs nanostructures is that the strong PZ field can be exploited for the fabrication of single photon emitters operating at elevated temperatures,[18] or sources of entangled photon pairs.[19] Until now, the majority of experimental work on high index surfaces has focused primarily on (N11) InAs/GaAs QDs with $N>2$. Therefore, it appears attractive to investigate the growth of self-organized QDs in the (211)B orientation in order to exploit the relatively larger PZ field in this direction.

In this work, following a preliminary report,[20] we investigate thoroughly the influence of various growth parameters on the structural and optical properties of InAs nanostruc-

a)Electronic mail: gdialyn@physics.uoc.gr.

tures grown by molecular beam epitaxy (MBE) on (211)B GaAs substrates. The structural analysis is based mainly on atomic force microscopy (AFM) images obtained on uncapped InAs nanostructures, and is corroborated by transmission electron microscopy (TEM) observations on a capped sample. We show that depending on the growth conditions, such as growth temperature, total amount of deposited InAs, and growth rate, the InAs nanostructures take the shape of a QD or a quantum dash (QDH), their height ranges from 2 to 20 nm, and their density can be as low as a few times 10^8 cm^{-2} and as high as a few times 10^{10} cm^{-2}. The InAs (211)B nanostructures have been optically studied by means of photoluminescence (PL) spectroscopy, based on which we demonstrate the formation of a two-dimensional (2D) wetting layer (WL), whose thickness is between 1 and 1.3 monolayers (MLs) in the (100) orientation, referred as MLs in the rest of the work (1 ML=0.303 nm). Furthermore, by analyzing the spectral position and linewidth of the PL QD emission, we reach the conclusion that only small size QDs are optically active. This conclusion is coherent with high resolution TEM (HRTEM) observations showing that large QDs contain dislocations, whereas small QDs are dislocation-free. Finally, we present clear evidence of the internal field present in these QDs.

II. EXPERIMENTAL DETAILS

For the purposes of this work, a total of 46 InAs QD samples have been grown by MBE on n^+ GaAs (211)B substrates under various growth conditions. After transfer to the MBE growth chamber the native oxide of the GaAs substrate is thermally desorbed by heating to ~580 °C under an As flux, while the background pressure during growth is 8×10^{-8} mbar. The growth process is monitored *in situ* by means of reflection high energy electron diffraction (RHEED), and the growth rate is determined from RHEED oscillation measurements on GaAs(001). A typical sample consists of a 0.5 μm thick nominally undoped GaAs buffer layer, grown at 620 °C, followed by the growth at the same temperature of a 40 period (2.3 nm GaAs/1.5 nm AlAs) superlattice (SL), which is known to produce a high quality template for the nucleation of InAs QDs, as well as to provide confinement of the photoexcited electron-hole pairs in the near surface region. Following the short-period SL, a thin 10 nm GaAs layer is grown, and then the growth temperature is ramped down to T_G=400, 450, 500, and 530 °C for the deposition of InAs. The effect of growth rate, G, on the shape and size of InAs nanostructures is investigated by using three different values of G=0.1, 0.048, and 0.0216 ML/s. Another crucial parameter for the formation of QDs is the amount of deposited InAs material, Θ, varied in this work between 0.7 and 3 MLs. For each set of growth conditions (T_G, G, and Θ), two samples are produced: one for AFM characterization where the InAs layer is left uncapped, and another for optical characterization where the InAs layer is capped by a 30 nm GaAs layer, grown at the same temperature as the InAs layer in order to avoid In segregation and interdiffusion effects. TEM samples in cross-section and plan-view orientations are prepared by mechanical grinding followed by precision Ar^+ ion milling to electron transparency. TEM observations are carried out in a HRTEM Jeol 2011 electron microscope, operated at 200 kV, with C_s =0.5 mm and point resolution 0.194 nm. The PL spectra are typically obtained at 18 K, using a He–Cd continuous wave laser at 325 nm as excitation, and a liquid nitrogen-cooled charge coupled device (CCD) camera as detector. Considering that according to theoretical calculations the InAs (211)B nanostructures produced in this work could possibly emit at longer wavelengths than the CCD's 1.1 μm cutoff, we have systematically scanned for PL emission down to 1.6 μm with the help of an InGaAs photodiode. However, in this work, no PL emission was observed beyond 1.1 μm for reasons that will become clear below.

III. RESULTS AND DISCUSSION

We first studied the effect of growth temperature by depositing on (211)B GaAs 2.5 MLs of InAs with a rate of 0.1 ML/s at 400, 450, 500, and 530 °C. In all cases, the RHEED pattern remains streaky during the initial growth stages of InAs, indicating the growth of a 2D InAs layer on GaAs. After a critical thickness, however, a drastic change in the RHEED pattern occurs marking the transition from 2D to three-dimensional (3D) growth mode and the formation of InAs nanostructures: for $T_G \leq 500$ °C, the pattern turns from streaky to spotty and InAs QDs are formed, as shown in the AFM images of Figs. 1(a) and 1(b). On the other hand, for T_G=530 °C a distinctly different RHEED pattern transition is observed, from streaky to hazy, suggesting the formation of another type of nanostructure. Indeed, as illustrated in Fig. 1(c), elongated QDHs are formed, with a typical size of 20 nm high, 200 nm long, and 100 nm wide. The QDH density (~10^9 cm^{-2}) is much smaller compared to QD samples, with no trace of coexistence of small dots on the sample surface. By carefully orienting Fig. 1(c), we conclude that dashes tend to nucleate and align along multiatomic steps oriented in the $[\bar{1}11]$ direction, indicating a lower surface energy at these sites. The formation of such steps on a (211)B GaAs surface has been reported previously.[21] Although in this work we focus primarily on QDs, it is interesting to note that similar alignment along multiatomic steps of (111)B-grown InAs nanostructures has been reported by us elsewhere.[22]

With increasing T_G the InAs nanostructures increase in size and their density decreases. This is illustrated in Fig. 2, showing the height distribution (upper part) and the total density of nanostructures (lower part) grown at different growth temperatures with Θ=2.5 MLs and G=0.1 ML/s. The mean height varies from 2.5 nm at 400 °C, to 4 nm at 450 °C, 9 nm at 500 °C, and 20 nm at 530 °C. Similarly, a striking decrease in the nanostructure density, by more than one order of magnitude, upon increasing the temperature from 400 to 530 °C is observed. This behavior, which is observed for lower growth rates as well, is consistent with the enhanced surface mobility of adatoms with increasing temperature. Adatoms migrate longer on the surface and site selectivity is enhanced, giving rise to larger dots. Moreover,

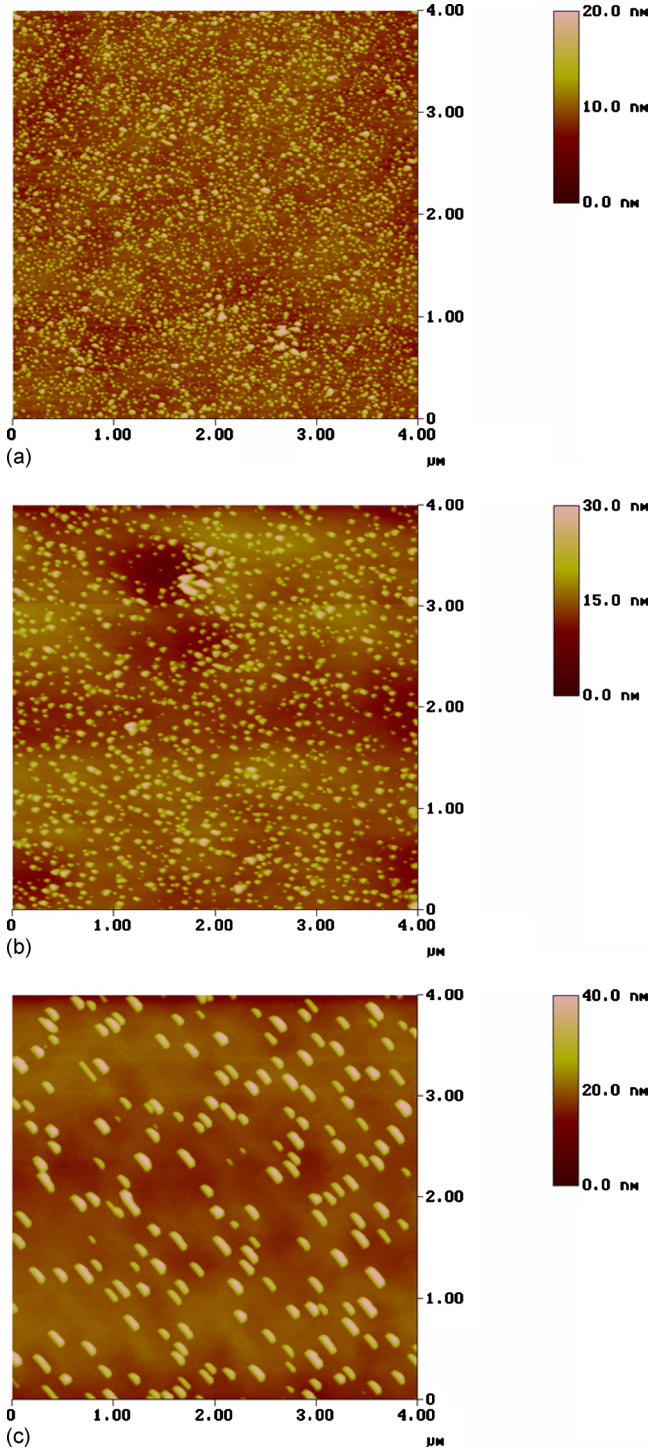

FIG. 1. (Color online) AFM images of InAs nanostructures grown on (211)B GaAs at different growth temperatures, (a) 450 °C (#603), (b) 500 °C (#601), and (c) 530 °C (#607). In all cases, Θ=2.5 MLs and G =0.1 ML/s.

as shown by TEM, large dots relax their strain by forming dislocations, facilitating the incorporation of additional adatoms and increasing further their size.

In Fig. 3(a), we compare the height distribution of two QD samples grown at different growth rates, with Θ =2.5 MLs and T_G=500 °C. A clear spreading of the distribution toward the large QD sizes is observed when the lower growth rate is employed. In keeping with this observation,

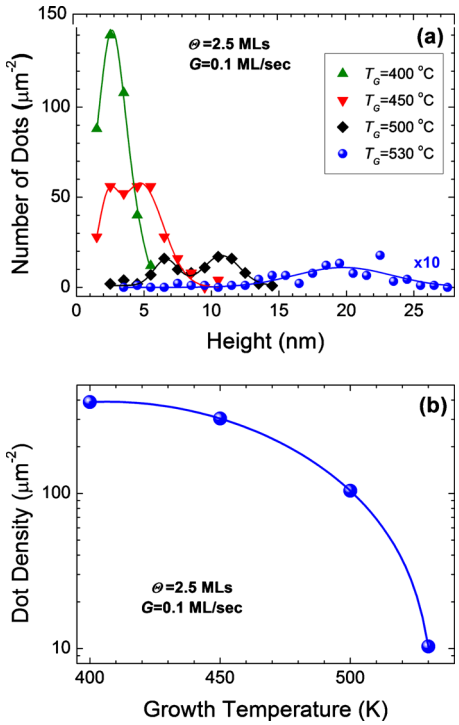

FIG. 2. (Color online) (a) Distribution of QD or QDH heights for various samples grown at 400 °C (#605), 450 °C (#603), 500 °C (#601), and 530 °C (#607), with Θ=2.5 MLs and G=0.1 ML/s. (b) Corresponding total dot density vs growth temperature. The lines through the data points are guides to the eye.

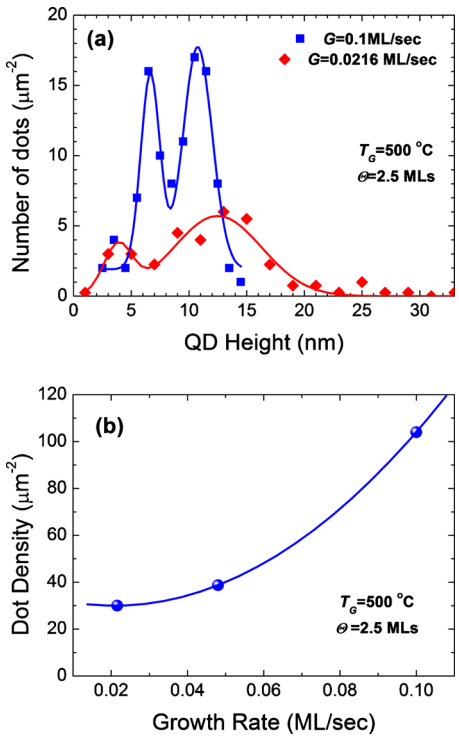

FIG. 3. (Color online) (a) Distribution of QD heights for two samples grown using different growth rates of 0.1 ML/s (#601) and 0.0216 ML/s (#619), with T_G=500 °C and Θ=2.5 MLs. (b) Total dot density as a function of growth rate. The lines through the data points are guides to the eye.

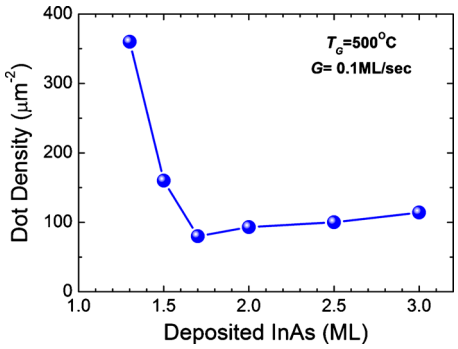

FIG. 4. (Color online) Total dot density in samples grown at T_G=500 °C with G=0.1 ML/s for various amounts of deposited InAs: Θ=1.3 ML (#691), Θ=1.5 ML (#669), Θ=1.7 ML (#689), Θ=2.0 ML (#667), Θ=2.5 ML (#665), Θ=3.0 ML (#663). The lines connecting the data points are guides to the eye.

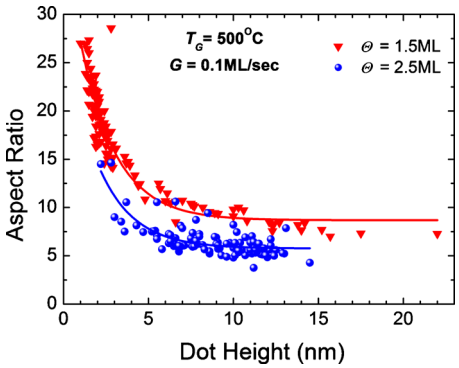

FIG. 6. (Color online) Aspect ratio as a function of height for QDs grown at T_G=500 °C with a rate G=0.1 ML/s, with Θ=2.5 MLs (circles, #601) and Θ=1.5 MLs (triangles, #669). The lines running through the data points are guides for the eye.

the dot density increases with the growth rate, as depicted in Fig. 3(b). Both observations can be understood considering the increased migration length of adatoms at lower growth rate conditions giving rise to fewer and larger QDs.

Another very critical growth parameter governing the morphology of InAs nanostructures is the amount of deposited InAs, Θ. To study this dependence, a series of samples with T_G=500 °C and G=0.1 ML/s was grown, by varying Θ between 1.3 and 3.0 MLs. It should be noted that for Θ <1.3 MLs, the InAs surface remains 2D and exhibits no formation of 3D islands. In Fig. 4, the nonmonotonic variation in the QD density with Θ≥1.3 MLs is plotted. For Θ =1.3 MLs, a clear Stranski–Krastanow transition occurs and small and dense 3D InAs islands are formed, with a typical height of 2 nm and a density of 3.7×10^{10} cm^{-2}. For Θ =1.5 and 1.7 MLs, a significant drop of the dot density is observed, down to $\sim10^{10}$ cm^{-2}, accompanied by the appearance of larger size dots. This can be attributed to coalescence of neighboring dots occurring in these conditions, leading to reduced dot densities. For Θ>1.7 MLs, however, the dot density remains practically constant, even though the QDs continue to grow in size, acting as nucleation centers and attracting the additional adatoms impinging on the surface. Apparently, this size increase is not uniform and occurs in a fashion that broadens the QD size distribution, as shown characteristically in Fig. 5, where we compare the QD height (H) and diameter (D) distributions of two samples with Θ =1.5 and 2.5 MLs. Clearly, a much narrower size dispersion is obtained for Θ=1.5 MLs, with the majority of QD heights being smaller than 3 nm, which is important since as we discuss below, only small QDs are optically active.

Additional information on the shape of the (211)B InAs QDs is obtained by extracting the diameter to height aspect ratio of the dots from the AFM data. In Fig. 6, we plot the aspect ratio as a function of dot height for the two samples presented in Fig. 5. For both samples, the aspect ratio appears to increase strongly with decreasing dot height, and for H<3 nm can easily reach values larger than 10. The dependence of aspect ratio on dot size is consistent with the theoretical analysis of Daruka *et al.*,[23] who have established that with increasing size the stable shape of islands evolves from platelets to truncated pyramids and then to full pyramids.

We complete the structural analysis of InAs QDs grown on (211)B GaAs by presenting TEM and HRTEM results on a capped QD sample (#597), grown at T_G=500 °C with G =0.1 ML/s and Θ=2.5 MLs. A bright field cross-section TEM image taken along [$\bar{1}$11] zone axis is presented in Fig. 7, in which the GaAs thin layer on top of the AlAs/GaAs SL and the InAs QDs capped with a GaAs layer are clearly visible. As seen, the QDs are relatively large, with sizes simi-

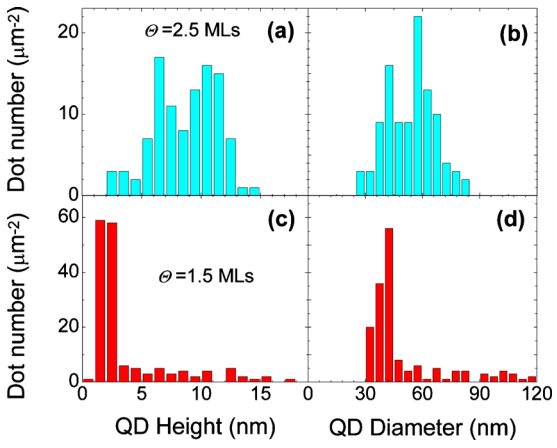

FIG. 5. (Color online) [(a) and (c)] Histograms of QD heights for two samples grown with T_G=500 °C and G=0.1 ML/s, with Θ=2.5 MLs (#601) and Θ=1.5 MLs (#669), respectively. [(b) and (d)] Histograms of QD diameters of same samples.

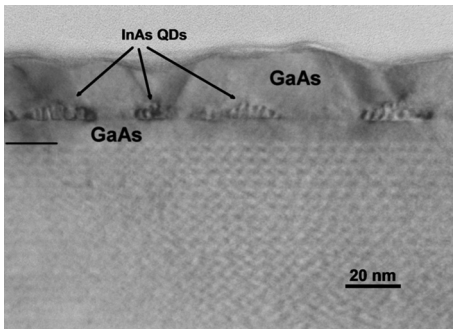

FIG. 7. Bright field cross-section TEM image, taken along [$\bar{1}$11] zone axis, showing the GaAs thin layer on top of the AlAs/GaAs SL and several InAs QDs of various sizes capped by the GaAs cap-layer.

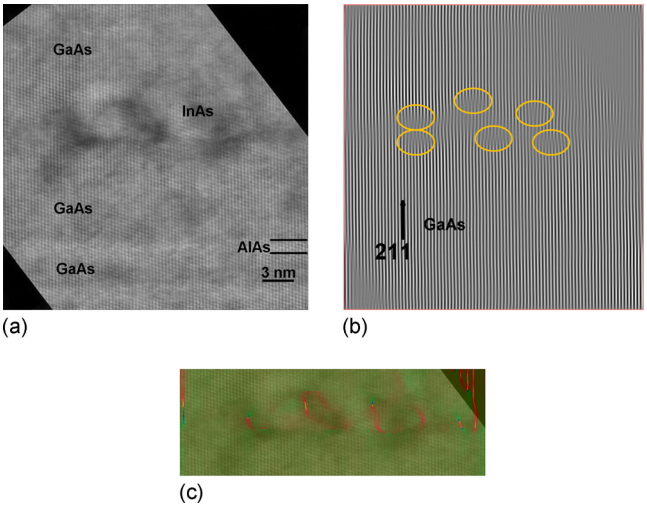

FIG. 8. (Color online) (a) HRTEM image from a large QD, with height 6 nm and base 16.5 nm, viewed along the $[01\bar{1}]$ zone axis. (b) The same image after Fourier filtering using the in plane 111 spatial frequencies, demonstrating the presence of misfit dislocations. (c) DDT map calculated from the HRTEM image of (a), superimposed to the image, indicating the location of the core of the misfit dislocations which delineate the QD.

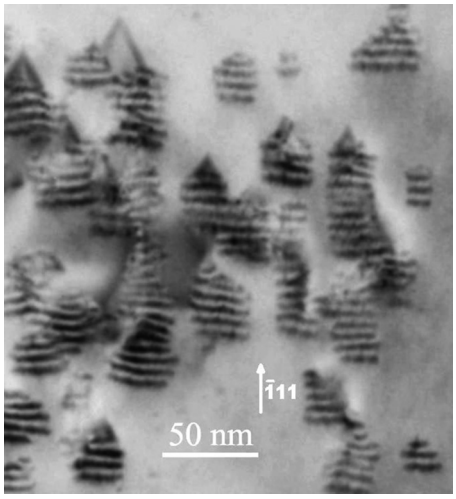

FIG. 9. Plan-view bright field TEM image, taken along [211] off-axis with $g=\bar{1}11$, showing the truncated pyramidal morphology of the QDs.

lar to those observed by AFM in uncapped QD samples grown under the same conditions. Figure 8(a) illustrates a cross-section HRTEM image from the same sample, viewed along the $[01\bar{1}]$ zone axis, depicting a large QD in this case with height equal to 6 nm and base 16.5 nm. The Moiré fringes which are visible on the dot, considering they are usually formed by the superposition of two mismatched structures, strongly suggest that the dot is at least partially relaxed. Further proof on the dot relaxation is achieved by directly "counting" the misfit dislocations, appearing as terminating extra-half planes (encircled) in the Bragg image of Fig. 8(b). Figure 8(b) is the Fourier filtered image of Fig. 8(a) using in-plane spatial frequencies. At this point, it is important to note that *no misfit dislocations* were detected in HRTEM observations of small dots, with $H \leq 3$ nm. In Fig. 8(c), the part of the image of Fig. 8(a) containing the QD, is shown superimposed by the dislocation density tensor (DDT) image map. The DDT is calculated from the HRTEM image by applying geometric phase analysis. DDT locates the core of the misfit dislocations which delineate the QD, since it takes nonzero values only at the dislocation core region.[24] Finally, Fig. 9 presents a plan-view bright field TEM image taken along [211] off-axis with $g=\bar{1}11$, the analysis of which clearly suggests a truncated pyramidal morphology for the QDs, in good agreement with the large aspect ratios reported in Fig. 6. The spacing of the Moiré fringes measured in the image is equal to 5.5 nm, leading to a d-spacing of the {111} lattice planes of InAs $d_{111\ InAs}=0.34495$ nm instead of 0.3498 nm which is the nominal relaxed value, suggesting that these particular QDs are partially relaxed.

We discuss now the optical properties of (211)B InAs nanostructures, in relation to their structural and morphological characteristics. In Fig. 10, we present typical low-temperature PL spectra from two samples containing QDs and QDHs, grown at $T_G=500$ °C and $T_G=530$ °C, respectively, with $G=0.1$ ML/s and $\Theta=2.5$ MLs. In both samples, the PL spectrum is dominated by a high energy peak at ~1.75 eV, not shown in the figure, which is due to radiative recombination at the GaAs/AlAs SL.[20] The weak shoulder at ~1.5 eV is near-gap emission from the n^+ GaAs substrate. In the QD sample, the PL peak associated with electron-hole recombination in the (211)B InAs QDs is the lower energy peak at 1.27 eV. A striking aspect of this peak is the relatively narrow linewidth of about 50 meV. This is unanticipated considering the broad QD size distribution expected for this sample, according to Figs. 5(a) and 5(b). Another interesting point is that the QD PL intensity of this sample is more than one order of magnitude weaker compared to equivalent (100)-oriented InAs QD samples typically grown by us. Both of these points are discussed in detail below. On the other hand, in the QDH sample, the PL spectrum contains only one prominent peak at ~1.40 eV. This peak cannot be attributed to QDH emission, since according to Figs. 1(c) and 2(a), the dashes in this sample are expected to have much larger volumes compared to the QDs. Therefore, if the QDHs emitted, their emission should be at much lower energy compared to the QDs, which is clearly not the case here. In addition, due to their large size (e.g., $H=18-20$ nm), the QDHs are most likely strain-relaxed by forming multiple dislocations and are thus not expected to

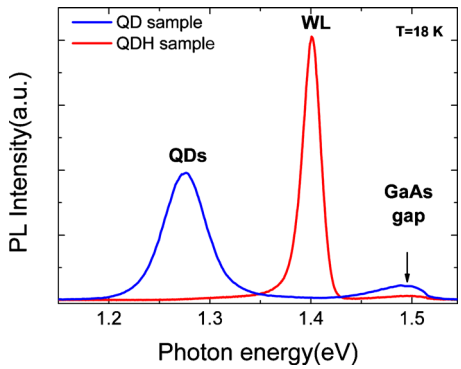

FIG. 10. (Color online) Comparison of PL spectra at T=18 K from a (211)B InAs QD sample grown at 500 °C (#602), and a QDH sample grown at 530 °C (#608).

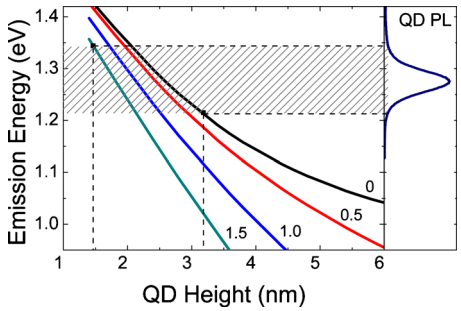

FIG. 11. (Color online) Calculated QD ground state energies as a function of island height for different values of the internal PZ field, ranging from 0 to 1.5 MV/cm. On the right hand side, the PL spectrum of the QD sample (#602) of Fig. 10 is shown. Shaded area represents the energy range of QD emission. By inspection, it is clear that, independently of the field value, the QD emission energies correspond to small QDs, with $H \leq 3$ nm.

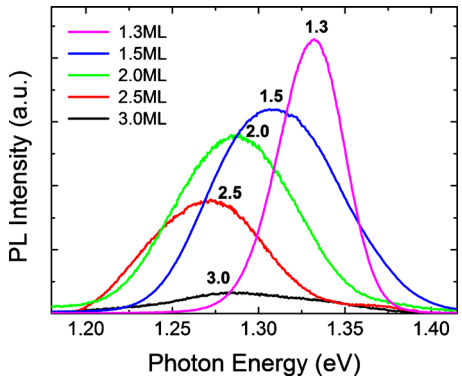

FIG. 12. (Color online) PL spectra at 18 K from (211)B InAs QDs grown at $T_G = 500$ °C with $G = 0.1$ ML/s, for various amounts of deposited InAs: $\Theta = 1.3$ ML (#692), $\Theta = 1.5$ ML (#670), $\Theta = 2.0$ ML (#668), $\Theta = 2.5$ ML (#666), and $\Theta = 3.0$ ML (#664). The three lower traces are multiplied by 10.

radiate. Therefore, we attribute the peak at 1.40 eV to PL emission from the InAs WL, which is simply enhanced in this case because of the low dash density ($\sim 10^9$ cm^{-2}), allowing for radiative recombination of electron-hole pairs in the WL, before being trapped in the QDHs.

In order to understand the QD emission spectrum of Fig. 10, we calculated the QD ground state energies as a function of QD height, assuming a one-dimensional (1D) Schrödinger equation model in the envelope function approximation. The 1D simplification is justified in our case by the large aspect ratio of the QDs, especially for small QD heights (see Fig. 6), implying that the quantum confinement along the growth direction is much stronger compared to the lateral dimensions. The PZ field inside the QDs was used as an adjustable parameter of the calculation. This was dictated by the vast uncertainty in the literature regarding the PZ field amplitude in the system. In Fig. 11, we plot the theoretical QD ground state energies as a function of QD height[25] for different values of the internal PZ field ranging from 0 to 1.5 MV/cm. By comparing the theoretical curves to the energy range of the QD PL emission, we conclude that, independently of the actual PZ field value, *the QD emission originates from small QDs*, with $H \leq 3$ nm. This conclusion is consistent with the HRTEM observations, where large QDs ($H = 6$ nm) were found to contain multiple dislocations, whereas small QDs ($H = 3$ nm) were found to be dislocation-free.

Realizing that only small dots ($H < 3$ nm) contribute to the QD emission can also explain the relatively weak PL of the QD sample of Fig. 10, compared to (100) counterparts. As shown in the histograms of Figs. 2(a) and 5(a), for its uncapped version (#601), the QD sample of Fig. 10 contains mostly large dots with an average height of ~ 8 nm. Therefore, only a small portion of dots participate in the PL emission of this sample, explaining its low PL efficiency. This interpretation is further supported by the results of Fig. 12, where we compare the PL spectra from a series of QD samples grown with $T_G = 500$ °C and $G = 0.1$ ML/s, by varying Θ between 1.3 and 3.0 MLs. As Θ decreases from 2.5 to 1.3 MLs, we observe a systematic blueshift in the QD emission, in good agreement with reduced average QD size and increased quantum confinement. Most importantly, however, with decreasing Θ, we observe a dramatic increase in the PL efficiency (please notice that the three lower curves are multiplied by 10). For example, between samples with $\Theta = 2.5$ and 1.5 MLs, the PL enhancement factor is ~ 20. This factor can be well accounted for considering that only small QDs, with $H < 3$ nm, radiate. Referring to the histograms of Fig. 5, obtained for the "uncapped" versions of the $\Theta = 1.5$ and 2.5 ML samples, we find that the percentage of dots with $H < 3$ nm are 75% in the $\Theta = 1.5$ ML sample and only 3% (i.e., a factor of 25 less) in the $\Theta = 2.5$ ML sample.

We turn now our attention to the estimation of WL thickness in our system. Toward this end, we examine a series of samples grown at 530 °C with varying Θ between 0.7 and 2.5 MLs. From RHEED measurements on these samples, we already know that for $\Theta < 1.3$ MLs, the InAs growth remains 2D, without any evidence of 3D nanostructures, whereas for $\Theta \geq 1.3$ MLs, a clear 2D–3D growth mode transition is observed, leading to the formation of QDHs. This implies that the critical thickness L_C for the 2D–3D transition is between 1 and 1.3 MLs, which automatically sets an upper bound for the WL thickness considering that $WL < L_C$. In order to obtain a more precise estimate of the WL thickness, we resort to the PL spectra obtained from these samples, shown in Fig. 13. All samples exhibit a pronounced PL peak

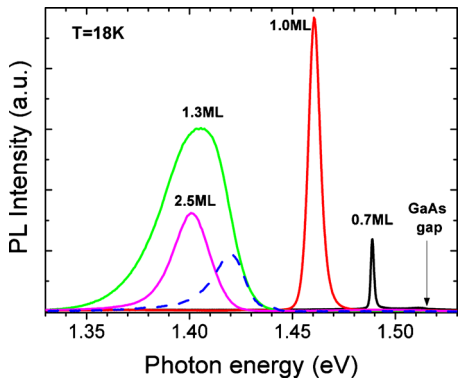

FIG. 13. (Color online) PL at 18 K from QDH samples grown at $T_G = 530$ °C with $G = 0.1$ ML/s for various amounts of deposited InAs: $\Theta = 0.7$ ML (#658), $\Theta = 1.0$ ML (#656), $\Theta = 1.3$ ML (#651), and $\Theta = 2.5$ ML (#608). The PL from the WL of a QD sample grown at $T_G = 450$ °C with G=0.0216 ML/s and $\Theta = 2.5$ ML (#623) is also shown in dashed line.

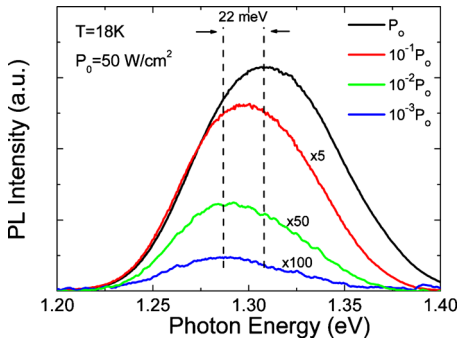

FIG. 14. (Color online) Excitation power dependence of PL emission from InAs QDs (#670) grown at 500 °C.

in the vicinity of the GaAs gap, whose spectral position depends strongly on Θ. Specifically, as Θ increases from 0.7 to 1.3 MLs, a pronounced PL redshift is observed from 1.49 down to 1.40 eV, as a result of reduced confinement in the InAs 2D layer. For $\Theta \geq 1.3$ MLs, however, this PL redshift is completely saturated, clearly indicating that the 1.40 eV PL peak originates from the WL formed during the 2D–3D growth transition. From these results, we can obtain a lower bound for the WL thickness, which now follows the relation $1.0 \text{ ML} < WL < L_C < 1.3$ MLs, where 1 ML=0.303 nm. It is interesting to note that the above estimate of WL thickness is consistent with theoretical calculations, based on the 1-D Schrödinger equation. According to these calculations the 1.40 eV emission peak corresponds to a WL thickness of 1.22 MLs, which is equivalent to 3 MLs in the (211)B growth direction. In Fig. 13, we also show in dashed line the WL PL spectrum from a QD sample grown at T_G=450 °C with a growth rate of G=0.0216 MLs/s and Θ=2.5 ML (#623), strongly suggesting that the WL thickness does not change much with growth rate and temperature.

Clear evidence for the existence of strong PZ field in the (211)B InAs QDs can be found in Fig. 14, where we present the excitation power dependence of a typical QD PL emission. Interestingly, the QD PL peak blue shifts by about 22 meV in this power range, which is mainly attributed to the screening of the PZ field by electron-hole pairs injected in the QDs. Part of this blueshift could be also attributed to occupation of higher energy QD states. However, such a mechanism is usually accompanied by pronounced broadening of the PL spectrum on the high energy side, which is clearly not the case here, where the PL peak shifts essentially as a whole, with only a small increase in the PL linewidth of 15% in this power range. Further indication of the PZ field in the (211)B QDs can be found in T=10 K time-resolved PL experiments (data not shown), where a decay time of 1.1 ns was measured, as compared to 0.86 ns measured in (100) QDs of comparable size. Please note that in the absence of PZ field, the oscillator strength in the (211)B orientation is expected to be larger than in (100), and shorter decay times are expected. Therefore, the longer decay time in the (211)B case is very likely due to the PZ field.

IV. CONCLUSION

In this work, we have carried out a systematic study of the influence of various growth parameters on the structural and optical properties of InAs nanostructures, grown by MBE on (211)B GaAs substrates. Depending on the growth conditions, the nanostructures may take the shape of a QD or a QDH, their height ranges from 2 to 20 nm, and their density varies between a few times 10^8 cm^{-2} up to a few times 10^{10} cm^{-2}. By analyzing the QD emission spectrum, we conclude that only small QDs, with heights less than 3 nm, are optically active. This is consistent with HRTEM observations showing that large QDs contain misfit dislocations, whereas small QDs are dislocation-free. The formation of a 2D WL is observed optically, and its thickness is determined to be between 0.30 and 0.39 nm. Finally, we attribute the large blueshift in the QD emission with increasing excitation power to the built-in PZ field present in these dots. The expected large amplitude of the internal electric field makes these nanostructures excellent candidates for the realization of novel optoelectronic devices such as high-temperature single-photon emitters.

ACKNOWLEDGMENTS

This work was co-funded by the European Social Fund and National resources through the program PYTHAGORAS. We thank M. Gurioli and A. Vinattieri at LENS for the time-resolved PL experiments.

[1] P. Bhattacharya, S. Ghosh, and A. D. Stiff-Roberts, Annu. Rev. Mater. Res. **34**, 1 (2004).
[2] M. Bayer, P. Hawrylak, K. Hinzer, S. Fafard, M. Korkusinski, Z. R. Wasilawksi, O. Stern, and A. Forchel, Science **291**, 451 (2001).
[3] L. Landin, M. S. Miller, M. E. Pistol, C. E. Pryor, and L. Samuelson, Science **280**, 262 (1998).
[4] A. J. Shields, Nat. Photonics **1**, 215 (2007).
[5] D. I. Lubyshev, P. P. Gonzalez-Borrero, E. Marega, Jr., E. Petiprez, and P. Basmaji, J. Vac. Sci. Technol. B **14**, 2212 (1996).
[6] M. Henini, S. Sanguinetti, L. Brusaferri, E. Grilli, M. Guzzi, M. D. Upward, P. Moriarty, and P. H. Beton, Microelectron. J. **28**, 933 (1997).
[7] S. P. Guo, H. Ohno, A. Shen, F. Matsukura, and Y. Ohno, Appl. Phys. Lett. **70**, 2738 (1997).
[8] S. Guo, H. Ohno, A. Shen, Y. Ohno, and F. Matsukura, Jpn. J. Appl. Phys., Part 1 **37**, 1527 (1998).
[9] S. Sanguinetti, A. Miotto, S. Castiglioni, E. Grilli, M. Guzzi, M. Henini, A. Polimeni, A. Patané, L. Eaves, and P. C. Main, Microelectron. J. **30**, 419 (1999).
[10] D. L. Smith and C. Mailhiot, Rev. Mod. Phys. **62**, 173 (1990).
[11] S. Sanguinetti, M. Gurioli, E. Grilli, M. Guzzi, and M. Henini, Appl. Phys. Lett. **77**, 1982 (2000).
[12] M. Gurioli, S. Sanguinetti, and M. Henini, Appl. Phys. Lett. **78**, 931 (2001).
[13] F. Widmann, J. Simon, N. T. Pelekanos, B. Daudin, G. Feuillet, J. L. Rouviere, and G. Fishman, Microelectron. J. **30**, 353 (1999).
[14] J. Simon, N. T. Pelekanos, C. Adelmann, E. Martinez-Guerrero, R. André, B. Daudin, and L. S. Dang, and H. Mariette, Phys. Rev. B **68**, 035312 (2003).
[15] G. Bester, X. Wu, D. Vanderbilt, and A. Zunger, Phys. Rev. Lett. **96**, 187602 (2006).
[16] J. S. Lee, M. Sugisaki, H. W. Ron, S. Sugou, and Y. Masumoto, Physica E (Amsterdam) **7**, 303 (2000).
[17] G. Deligeorgis, G. Dialynas, Z. Hatzopoulos, and N. T. Pelekanos, Appl. Phys. Lett. **90**, 121126 (2007).
[18] J. Renard, R. Songmuang, C. Bougerol, B. Daudin, and B. Gayral, Nano Lett. **8**, 2092 (2008).
[19] A. Schliwa, M. Wilkelnkemper, A. Lochmann, E. Stock, and D. Bimberg, Phys. Rev. B **80**, 161307(R) (2009).
[20] M. Zervos, C. Xenogianni, G. Deligeorgis, M. Androulidaki, P. G. Savvidis, Z. Hatzopoulos, and N. T. Pelekanos, Phys. Status Solidi C **3**, 3988 (2006).

[21]T. Suzuki, Y. Temko, M. C. Xu, and K. Jacobi, Surf. Sci. **573**, 457 (2004).
[22]G. E. Dialynas, A. Pantazis, Z. Hatzopoulos, M. Androulidaki, K. Tsagaraki, G. Konstantinidis, C. Xenogianni, E. Trichas, S. Tsintzos, P. G. Savvidis, and N. T. Pelekanos, Int. J. Nanotechnol. **6**, 124 (2009).
[23]I. Daruka, J. Tersoff, and A.-L. Barabasi, Phys. Rev. Lett. **82**, 2753 (1999).
[24]J. Kioseoglou, G. P. Dimitrakopulos, P. Komninou, T. Karakostas, and E. C. Aifantis, J. Phys. D: Appl. Phys. **41**, 035408 (2008).
[25]Strictly speaking, in the 1D model of Fig. 11, the WL thickness is "hidden" in the QD height. However, this makes no big difference since, as we show in the analysis of Fig. 13, the WL is smaller than 0.39 nm.